Performance of a High Solar Fraction District Heating System

Tongjie Xu[1], Shai Li[1], Xuefeng Jiao[2], Kaichun Li[1], Qingtai Jiao[1], Jingshan Zhang[1]

[1] Sunrain Group Co., Ltd, Lianyungang (China)

[2] Northern Arizona University, Flagstaff (USA)

Abstract

At the end of 2019, a solar district heating system was built in Zhongba town in the west of Tibet. The system includes 32,175 m^2 of flat plate collectors, 15,000 m^3 of storage tank, 103,000 m^2 of heating area, and a 200-kW PV system. In the 2020-2021 heating season, the solar fraction of the system is 100%. This paper introduces the system characteristics, principles, and running situations and compares the simulated system performance with measured including solar fraction, collector efficiency. The collector array efficiency analysis method is discussed, the storage stratification is shown, and the heat loss factor is defined. The system has a good performance and proves that a high solar fraction district heating system is available in cold and high-altitude areas.

Keywords: Solar district heating, High Altitude, High Solar Fraction, Zhongba,

1.Introduction

The weather is freezing in Zhongba of Tibet, China, where the lowest temperature is lower than -40 degrees, and there is no reliable space heating during the eight months of frigid winter. There is no oil and gas there, and the primary heating material has been cow dung, which is not comfortable for users and is harmful to the environment. Considering the shortage of conventional sources and the rich solar energy, a high solar fraction district heating system was built to solve the heating problem. The construction was started in May 2019, and the system was put into operation in November 2019.

Fig. 1: Location of Zhongba (Source: Google Map)

2.System Description

2.1. System Overview and Parameter

With a total population of about 5,000 people, Zhongba has a total heating floor area of 103,000 m^2, including schools, hospitals, government offices, and residential houses. Carbon steel underground pipeline is laid along the side of the road. The altitude of Zhongba is 4700 m, which means the water will be boiled if the temperature is higher than 85°C if no additional pressure. For safety, low-temperature hot water heat-supply system is designed in Zhongba. The main design parameter is given in Table 1.

Tab. 1: Main design parameter

© 2021. The Authors. Published by International Solar Energy Society
Selection and/or peer review under responsibility of Scientific Committee
doi:10.18086/swc.2021.28.02 Available at http://proceedings.ises.org

Heating period	Total heat load (Design temperature)	Design solar fraction	Supply/return temperature in the city grid
Nov 1 to 31, May (251 days)	5.8MW (- 21.1°C)	95%	65/35 °C

High-efficiency flat plate collectors are used with 2340 pieces in total, taking up 32,175 m^2 of total aperture areas. The volume of the storage tank is 15000 m^3, and the diameter is 28.5 m. Meanwhile, 200 mm glass wool is used for insulation on the side, and 300 mm glass wool is used for insulation on the top.

A 1300 m^2 building was built for all equipment, including auxiliary heat sources with two sets of 1.4 MW diesel boilers, pump stations, heat exchange units, power distribution systems, and generators. Considering the lack and instability of local power, 200 kW photovoltaic power generation has been built, which is used in conjunction with municipal power and diesel generators. To solve the overheating problem, the system is equipped with three sets of 2 MW dry coolers. The project view is shown in Figure 2.

Fig. 2: Aerial view of the project

2.2. Brief Introduction of System Operation Logic

The system schematic is shown in Figure 3. When the solar radiation reaches a specific value or the temperature in collectors is higher than certain degrees, the solar circulation system will start to transfer heat to the tank. The speed of pumps is controlled by solar radiation to make the outlet temperature of solar collectors more stable. Hot water for space heating will come from the top of the tank. If the forward temperature is high enough, the water from the top of the tank will be mixed with water returned from the city grid or water in the middle of the tank to make the forward temperature stay at a suitable value. When the water temperature in the tank is low enough, the oil boilers start to work.

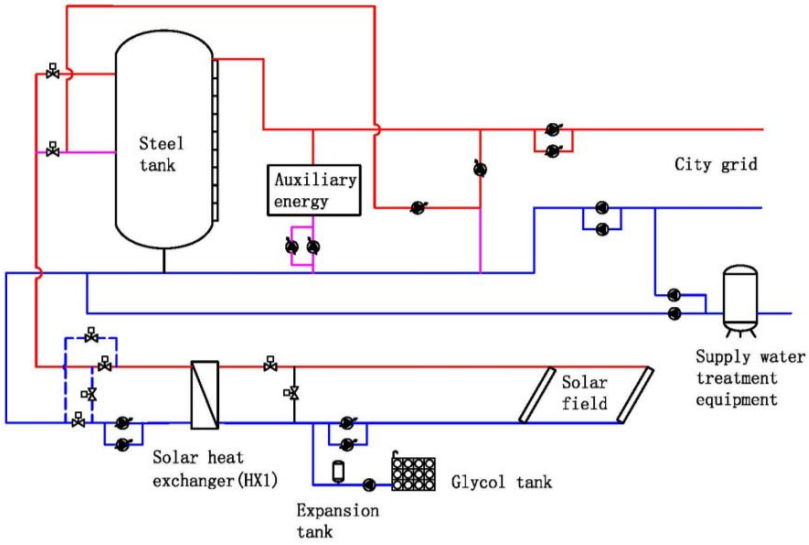

Fig. 3: System schematic diagram

The system is equipped with dry coolers to dissipate heat when the system is overheated. It is dangerous when the

bottom of the tank is at a high temperature. The system will start the protection mode to discharge heat by the solar collectors at night. When the temperature in the collector or the ambient temperature is lower than the set value, the antifreeze protection will start to work. The schematic system diagram is shown in Figure 3.

3.System performance

During the project design phase, an EnergyPro model and excel sheet models were developed to simulate the system, including solar fraction, collector efficiency, and heat load of the district heating system. Using 30 years of average historical weather data as a basis, the simulation model predicted that the system would provide more than 95% of the heating energy by solar. The average solar collector efficiency is more than 45.9%.

The system started to run in November 2019, and the performance of the system has been monitored since then by using its automatic control and data acquisition system. In practice, about 75% heating area was running in the 2019-2020 heating season. In the 2020-2021 heating season, 100% of the system was running. Since the system is designed as a high fraction, some collectors should be covered in non-heating months and low heating demand days (mainly in October, April, and May). Figure 4 is the comparison from November to March, which has almost no cover collectors. The average annual collector efficiency is about 47.8% compared with the predicted collector efficiency of 45.9% based on the gross area of the collectors, which means the current calculation method is relatively accurate.

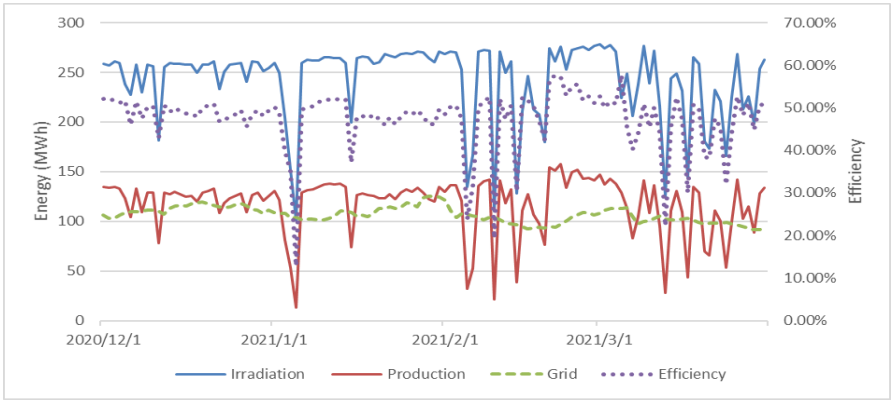

Fig. 4: System production

The actual solar fraction was 100% compared to the predicted 95%. After analyzing the calculation, actual solar radiation is about 10% higher than historical weather data in January and February. Another reason is that the local solar radiation is intense, and there will be some heat going into the house through big windows from 11:00 a.m. to 5:00 p.m. in the daytime. This heat should not be ignored in future designs.

4.Solar field performance

4.1. Collector and Array

Collectors of each gross area are 15.00 m^2, and apertures of 13.75 m^2 are applied in the Zhongba project. The efficiency from the supplier is below,

$$\eta=0.85-(2.3*(T_m-T_a))/G-(0.029*(T_m-T_a)^2)/G \qquad \text{(eq. 1.1)}$$

Harp collectors are chosen for this system and connected in series to form a collector row, while the absorber pipes of each collector are arranged in parallel.

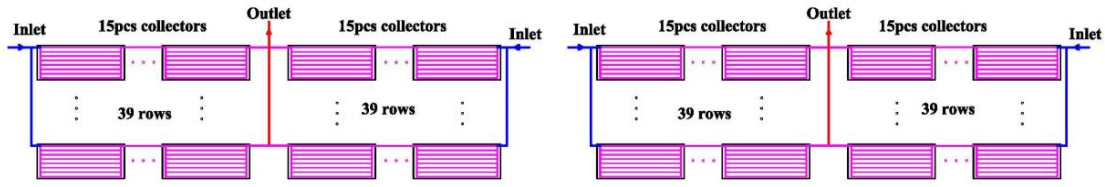

Fig. 5: Collector array schematic diagram

Each row has 60 pcs collectors, where 15 pcs collectors are connected in series, and two series share the same outlet pipes to reduce heat loss and system investment.

A non-Tichelmann connection is applied, and a balance valve from the IMI company combined with adjustments of pipe diameters is designed to reach homogeneous flow distribution (see Figure 3). The valve is calculated by Hyselect and precisely regulated.

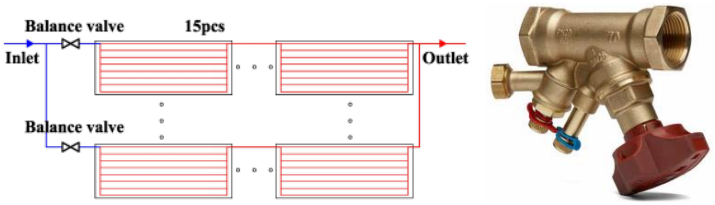

Fig. 6: Balance valve and arrangement diagram

4.2. Solar Irradiation

The solar field flow rate is controlled by irradiation in the Zhongba system. Nine solar irradiation sensors are divided into three groups are installed in different positions of solar field to reduce measure deviation. SP214-SS from Apogee company is used and fix in frame of collector.

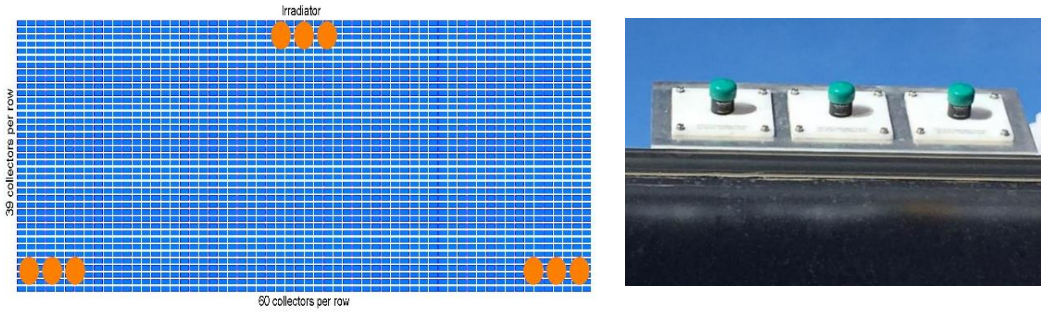

Fig. 7: Irradiation sensor and arrangement diagram

Zhongba is located at 29.762°N latitude and 84.032°E longitude and adopts GMT+8:00, which causes the sun to rise after ten o'clock and goes down around seven o'clock in winter. Several typical randomly selected kinds of weather are chosen to analyze the irradiation.

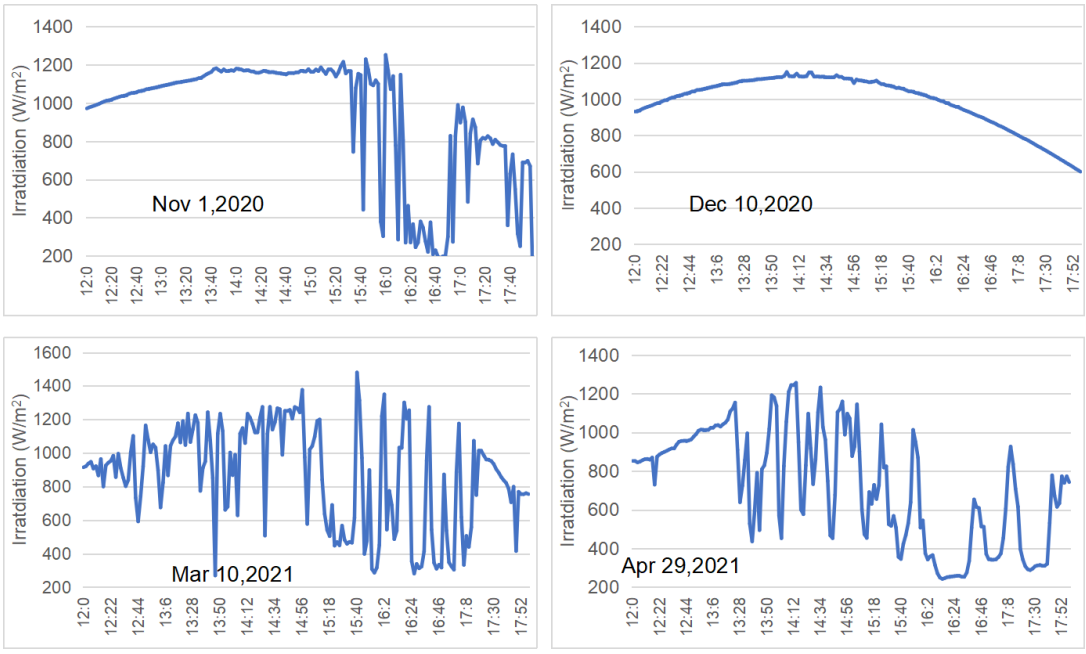

Fig. 8: Typical day irradiation in Zhongba (2 min interval)

The radiation value is relatively high, sometimes even exceeding the solar constant. The possible reason is that clouds and mountains bring transient scattering intensity to increase the radiation value. Because the radiation sensor, instead of the radiation meter, is used in this project, measurement accuracy cannot be promised. The reasons should be

further studied. It also can be found that the local radiation is very unstable, and it is difficult to find a relatively stable period for accurate analysis of the radiation and system performance.

4.3. Sensor Layout

Some sensors and measured parameter values are introduced to analyze the system better.

(1) Irradiation (G): According to the arrangement described in chapter4.1, the average value of nine measured values is usually taken as the radiation value G. If a sensor fails, the system will judge and eliminate the measured value of the faulty sensor. Because irradiation sensor measurement deviation and uncertainty value are relatively large, the controller will correct the irradiation value and flow rate to ensure that the outlet temperature of the solar field reaches the set value.

(2) Collector inlet and outlet temperature (T_{in}, T_{out}): Total of 16pcs sensors with 8 pcs inlet and 8 pcs outlet sensor of type 7403A1A from PR company are applied in the system.

(3) Average collector temperature T_m: The average inlet and outlet temperature

$$T_m=(T_{in}+T_{out})/2 \quad \text{(eq. 1.2)}$$

(4) Ambient temperature (Ta): Two ambient temperature sensors are installed in the solar field, using type 7403 from the PR company.

(5)Inlet and outlet temperatures of solar field heat exchanger ($Th_{x,\ in}$, $Th_{x,\ out}$): The energy from the solar field is passed through the heat exchanger (HX1), the inlet temperature is defined as $Th_{x,\ in}$, and the outlet temperature is defined as $Th_{x,\ out}$. Type 7403A1A from the PR company is applied in the system.

(6)Total flow of solar field (q_{sol})：

In order to better control the flow through irradiation, a flow sensor is installed in the main pipe, which indicates the total flow of the solar field. Type MAG5000+ MAG310P from Siemens is adopted.

(7) System production (P_{pro}):

As the heat collection field of this project uses antifreeze, it is not possible to directly set up a heat meter in the heat collection field. Therefore, a heat meter is installed on the secondary side of the heat collector plate (the medium is water). The heat meter type is Multical 801 from KAMSTRUP company.

4.4. Array Efficiency Analysis Method

At present, there is no unified standard for the testing of collector arrays. Meanwhile, the systems measure mainly depends on the system operation requirements, which means some value cannot get from this system. This paper will apply four different methods to analyze and compare the efficiency of the collector array.

(1) Based on the theoretical efficiency of the collector: Calculated by Equation 1.1, which is defined as η1 here.

(2) Based on the heat at the inlet and outlet of the collector: Here is defined as η2

$$\eta 2=c\rho q_v\Delta t_1/(3.6GAc) \quad \text{(eq. 1.3)}$$

Where

c: Specific heat capacity of propylene glycol, calculated by equation 1.4 [J/kg/°C]

ρ: Density of propylene glycol, calculated by equation 1.5 [kg/m^3]

q_v: Total circulating flow of heat collecting field [m^3/h]

Δt_1: The temperature difference between the inlet and outlet of the collector, $\Delta t_1=T_{out}-T_{in}$ [°C]

G: Solar radiation [W/m^2]

A_c: Total area of the heat collecting field, the project is 32,175 m^2

The manufacturer generally calculates the specific heat and density of propylene glycol-based on the equation fitted by the measured data. This project uses 45% propylene glycol, and its value at different temperatures is as equations 1.4 and 1.5.

$$c= 3633.48+203.59*T_m/100+93.54* T_m /100* T_m /100 \quad \text{(eq. 1.4)}$$

$$\rho= (1045.47-51.91* T_m /100-16.69* T_m /100* T_m /100) \quad \text{(eq. 1.5)}$$

Where T_m is calculated by Equation 1.2.

(3) Based on the heat of the primary side of the HX1: Here is defined as η3

$$\eta 3=c\rho q_v\Delta t_2/(3.6GA_{c)} \quad \text{(eq. 1.6)}$$

This calculation method is the same as equation 1.3. The difference is that the temperature difference is taken from the temperature difference between the inlet and outlet of the primary side of the heat exchanger. $\Delta t2=Th_{x,in}-Th_{x,out}$

(4) Based on plate exchange secondary side heat: Here is defined as η4

$$\eta 4=P_{field}/(G.A_c) \quad \text{(eq. 1.7)}$$

η_1 is the theoretical efficiency of the collector, while the project is installed by multiple sets of collectors in series and parallel. The measured value of the theoretical efficiency and the actual collectors' array efficiency has a big difference in irradiation, wind speed, and flow speed. Therefore, the difference between the collector and array efficiency is also an important content of this paper.

η_2 uses the inlet and outlet temperature directly from the collector array to calculate the efficiency. This temperature value is more suitable for measuring efficiency. However, due to the limited number of temperature sensors in the project, and it is impossible to set the flow sensor at the specific collector array, there may be uneven flow distribution, which may cause deviations in the calculated efficiency. At the same time, the density and specific heat capacity of propylene glycol apply the average temperature and fitted equation. Therefore, the deviation of the efficiency calculation may be further exacerbated.

η_3 calculates the efficiency using the flow rate and temperature difference of the primary side of the heat exchange (HX1). The measured temperature difference can be considered the comprehensive temperature difference of the entire solar field, but the deviation of propylene glycol's density and specific heat capacity is still unavoidable. At the same time, the measured efficiency is affected by the heat loss of the field pipeline and heat exchanger unit.

η_4 adopts the heat energy meter's measured value on the secondary side of the heat exchange (HX1). The medium on this side is water, so the calorific value is more accurate. However, the efficiency of the measurement is affected by the loss of the pipeline, the loss in the unit, and the logarithmic temperature difference of the exchanger. This value can reflect the solar field power more accurately, but there is a deviation for the collector array efficiency.

4.5. Collector Array Efficiency

It is impossible to measure and calculate the collector array efficiency accurately based on the current system conditions. Therefore, this paper will compare and analyze different measurement methods, hoping to provide ideas for accurate measurement in the future.

In order to ensure better measurement and analysis, it is necessary to select a period with slight radiation fluctuation and no collector covering. Here is the data from December 1, 2020.

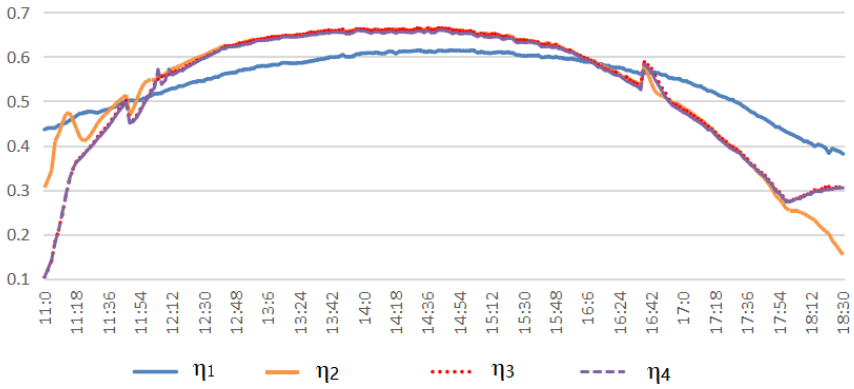

Fig. 9: Comparison of different efficiency (2 min interval)

The corresponding irradiation and the average temperature of the collector are shown in Figure 10.

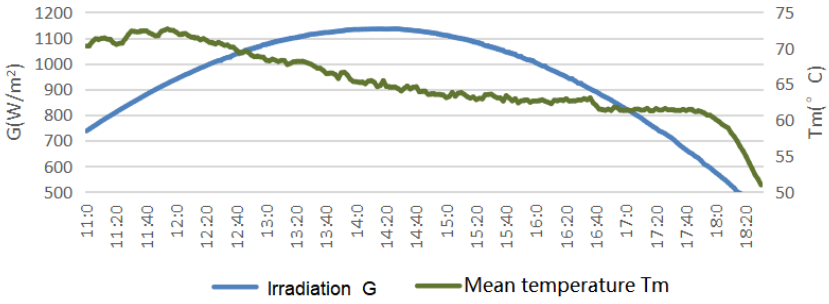

Fig. 10: Corresponding irradiation and average temperature (2 min interval)

It can be found that the measured values of η_2, η_3, and η_4 are almost the same when the irradiation is high, and they are all higher than the theoretical calculation values η_1, which reflects the excellent performance of the collector array and small heat losses of pipes and units.

The curves of η_3 and η_4 are the same, reflecting that the logarithmic temperature difference of heat exchange has little effect on the heat collection efficiency, mainly because this project adopts two parallel exchanges operated simultaneously. The designed logarithmic temperature difference temperature is only 3ºC.

In the case of high irradiation, the values η_1, η_2, η_3, and η_4 are all greater than 60%, the highest of η_2, η_3, and η_4 is even up to 66%, which is greater than expected. It also reflects the possible problems with the current measuring and calculation method of heat collection efficiency. There may be several reasons. First, the project uses an irradiance sensor rather than a highly accurate irradiance meter which will cause the calculation efficiency to be significant. Second. This project uses nine different irradiation sensors to take the average value. The value is not enough to reflect the accurate irradiation of the entire solar field. The calculated efficiency will also be too large if the calculated irradiance value G is smaller than the actual value. Third, the sensors in the project only ensure the system's operation but cannot perform accurate measurements. The errors of sensors will also affect the final value.

After further analysis of the above data, it can be found that when the irradiation intensity is low, the theoretical value is greater than the actual value. This is because of the effect of irradiation on efficiency, and on the other hand, low irradiation occurs in the morning and evening. Furthermore, the theoretical calculation efficiency does not consider the influence of the incident angle on the measured value, which causes deviation. When the radiation intensity is high, the actual measured efficiency is higher than the theoretical efficiency, reflecting the collector's excellent performance under high radiation conditions.

5.Tank performance

5.1. Tank Introduction

The project uses steel tanks as heat storage which also undertakes the supply pressure for the city grid. In this way, installing a heat exchanger on the city gird is unnecessary, which can reduce the temperature loss and improve the collector's efficiency.

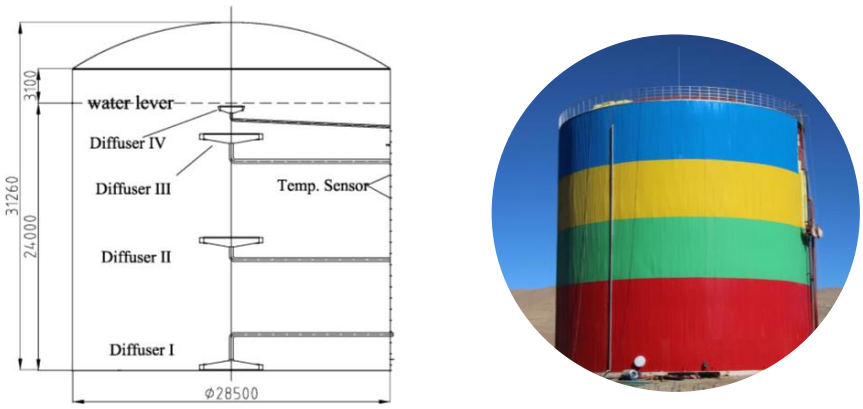

Fig. 11: Steel tank and overall dimensions

Steel tanks are adopted as heat storage which also provides city grid pressure. In this way, installing a heat exchanger

on the city gird is unnecessary, which can reduce the temperature loss and collector efficiency.

There are four diffusers in the tank. Diffuser I is connected to solar field supplying and city gird returning. Diffuser II is for the mid-temperature solar system, while Diffuser III is for the high temperature. The diffuser is just simply designed based on the best cost-performance ratio instead of best stratification. Anyhow it shows good performance where temperature difference between top and bottom reach nearly 40°C. Here is the temperature on Dec.1, 2020.

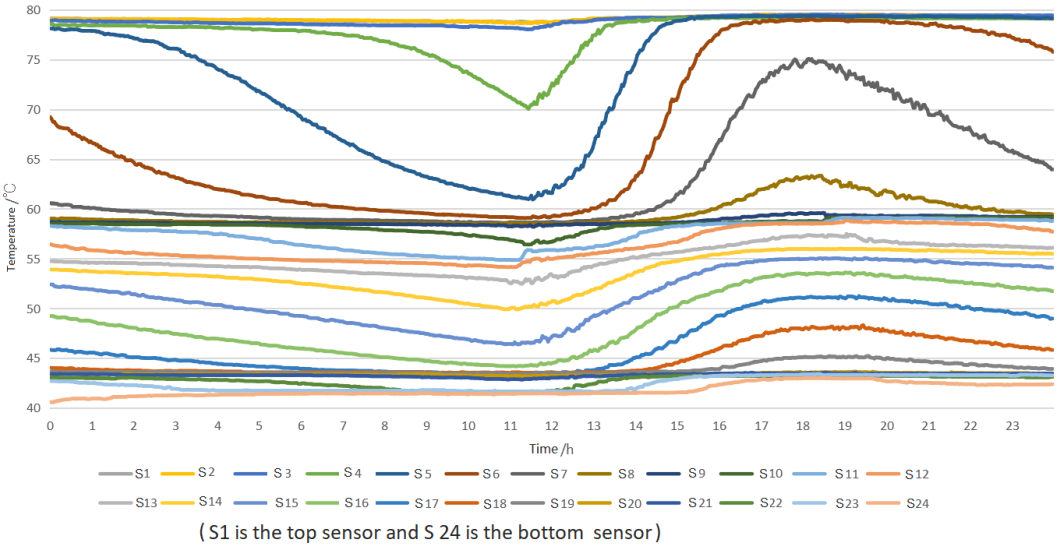

Fig. 12: Steel tank stratification on one day

5.2. Average Heat Loss Factor

Regarding the Chinese standard GB/T 28745-2012, the heat loss factors of steel tanks can be defined as

$$U_L = \frac{\rho_w c_w}{\Delta\tau} \ln\left[\frac{\sum_{i=1}^{n} t_i / n - \sum_{j=1}^{m} t_j / m}{\sum_{f=1}^{n} t_f / n - \sum_{j=1}^{m} t_j / m}\right] \qquad \text{(eq. 1.8)}$$

Where

U_L: Average heat loss factor [W/m^3/K]

ρ: Fluid density [kg/m^3]

c: Fluid specific heat capacity [J/kg/°C]

Δτ: Measurement time [s]

t_i: Initial temperature [°C]

n: Number of sensors

t_j: Average daily ambient temperature [°C], which can be measured and calculated every day.

m: Measurement day time

t_f: Finished temperature [°C]

This equation is only applicable to steel tanks whose sensor position is evenly distributed along with the height, and the tank is a cylindrical structure with the same diameter up and down.

During the heating season, the tank will charge and discharge every day and every minute. It is hard to measure and calculated the data. Several days after the system is stopped, the tank temperature can be relatively stable. Here in the table is the data from July 1 to August 7.

Tab. 2: Tank temperature from July 1 to August 7 (S1 is the top sensor, S24 is the bottom sensor)

Sensor	1-Jul (°C)	7-Aug (°C)	Sensor	1-Jul (°C)	7-Aug (°C)	Sensor	1-Jul (°C)	7-Aug (°C)
TT. S1	52.99	49.36	TT. S9	48.63	49.37	TT. S17	42.72	42.04
TT. S2	52.99	49.38	TT. S10	46.49	46.5	TT. S18	42.51	41.76
TT. S3	52.98	49.35	TT. S11	46.11	45.57	TT. S19	42.1	41.32
TT. S4	52.91	49.24	TT. S12	45.98	45.2	TT. S20	41.2	40.71
TT. S5	52.99	49.41	TT. S13	45.62	44.59	TT. S21	40.92	40.33
TT. S6	52.99	49.35	TT. S14	44.75	43.9	TT. S22	40.73	39.67
TT. S7	52.9	49.31	TT. S15	43.49	42.93	TT. S23	40.71	38.21
TT. S8	50.93	49.3	TT. S16	43.11	42.41	TT. S24	37.72	33.04

The ambient temperature is measured in hours. Here is the average everyday temperature, and the total mean temperature from July 1 to August 7 can be calculated, which is 12.26°C.

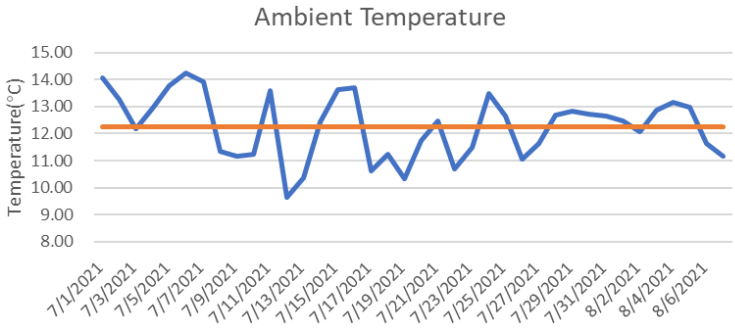

Fig. 13: The ambient temperature from July 1 to August 7

The average heat loss factor is U_L=0.0673 W/m^3/K. We can simulate the system performance by day or by the hour with this data, considering the tank heat loss. U_L is also an essential parameter for steel tank evaluation.

6.PV System Performance

Zhongba has not been connected to the national grid before. Therefore, a 200-kW photovoltaic system working with a 372-kWh battery and a diesel generator is chosen to meet system and domestic electricity demand.

According to data on December 19, 2020, the PV panel started working from around 7:40 and gradually increased. The photovoltaic power was less than the load before 08:30, which brings the battery discharging. After that, the photovoltaic power is greater than the load, and the extra power is supplied to the battery. From 11:10 to 13:30 and after 13:30, a similar phenomenon happens again until 16:30.

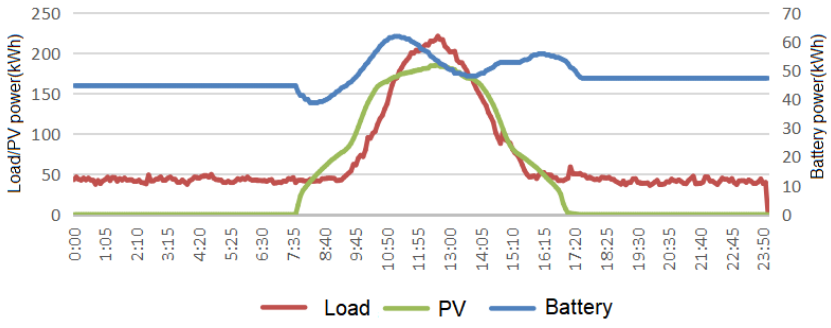

Fig. 14: PV system data on December 19, 2020

Here we choose the whole 2020 year. From January to December 2020, the total photovoltaic power generation capacity is 260711 kWh. It can save savings about 181,194 CNY based on Tibet electricity price of 0.695 yuan/kWh, while saves 651,778 CNY if all electricity is supplied from diesel generators, which is about 2.5 yuan/kWh in Zhongba. The PV system return on investment can reach 3-8 years in Zhongba.

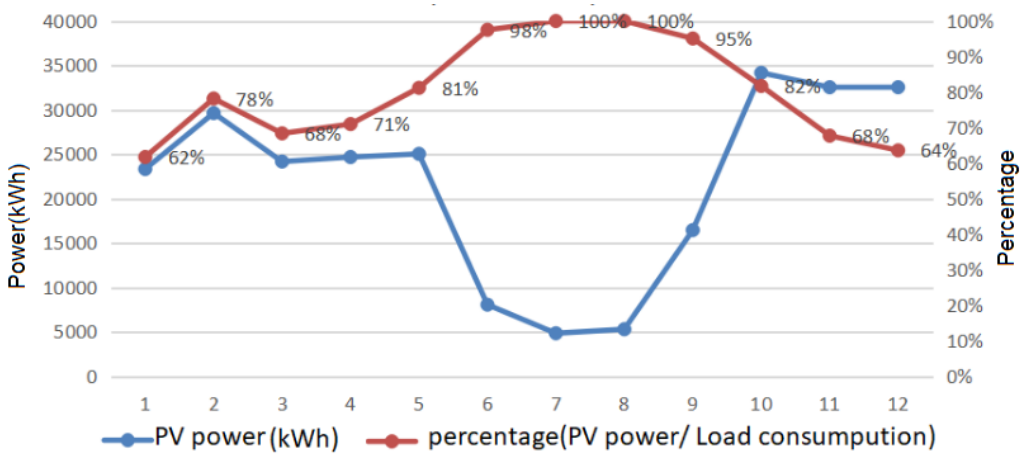

Fig. 15: PV system in 2020

In 2020, the average power supply of photovoltaic energy storage systems will account for 74%. The photovoltaic has a high degree of consistency with the solar heating system's power demand, but the battery is still required for regulation if no city power.

7.Conclusion

The system meets the design requirements through the analysis of one year's operation. The solar field and heating load are consistent with the design. The success of this project also proves the feasibility and economic value of a high solar fraction district heating system in cold and high-altitude areas.

Four different methods are given and compared to measure the array efficiency, but the best method is still required in the future. The collector array appears to have good performance and even more than expected, but there may be some error in the measured data, which should be further analyzed.

The heat loss factor is introduced by evaluating the steel tank insulation performance. Maybe a more reasonable index can be applied in the future.

PV system appears to have good performance as expected. PV system can be nearly 100% supply for solar heating system operation if the loaded power is calculated and predicted in more detail, and the battery is well proportioned with PV power,

8.References

Jiao, Q., Li, S., Gao, F., Wang, W., Qin, K., 2020. The Performance of a High Altitude and High Solar Fraction Large- Scale District Heating Project. SWC2019/SHC2019.

Mesquita, L., McClenahan, D., Thornton, J., Carriere, J., Wong, B. 2017. Drake landing solar community: 10 years of operation. ISES conference proceedings.

Sibbitt, B. et al.., 2007. The Drake Landing solar community project: Early results.